CT Kernel Conversion Using Multi-domain Image-to-Image Translation with Generator-Guided Contrastive Learning

Changyong Choi[1,2], Jiheon Jeong[1,2], Sangyoon Lee[2], Sang Min Lee[3], and Namkug Kim[2,3(✉)]

[1] Department of Biomedical Engineering, AMIST, Asan Medical Center, University of Ulsan College of Medicine, Seoul, Republic of Korea

[2] Department of Convergence Medicine, Asan Medical Center, University of Ulsan College of Medicine, Seoul, Republic of Korea
namkugkim@gmail.com

[3] Department of Radiology, Asan Medical Center, University of Ulsan College of Medicine, Seoul, Republic of Korea

Abstract. Computed tomography (CT) image can be reconstructed by various types of kernels depending on what anatomical structure is evaluated. Also, even if the same anatomical structure is analyzed, the kernel being used differs depending on whether it is qualitative or quantitative evaluation. Thus, CT images reconstructed with different kernels would be necessary for accurate diagnosis. However, once CT image is reconstructed with a specific kernel, the CT raw data, sinogram is usually removed because of its large capacity and limited storage. To solve this problem, many methods have been proposed by using deep learning approach using generative adversarial networks in image-to-image translation for kernel conversion. Nevertheless, it is still challenging task that translated image should maintain the anatomical structure of source image in medical domain. In this study, we propose CT kernel conversion method using multi-domain image-to-image translation with generator-guided contrastive learning. Our proposed method maintains the anatomical structure of the source image accurately and can be easily utilized into other multi-domain image-to-image translation methods with only changing the discriminator architecture and without adding any additional networks. Experimental results show that our proposed method can translate CT images from sharp into soft kernels and from soft into sharp kernels compared to other image-to-image translation methods. Our code is available at https://github.com/cychoi97/GGCL.

Keywords: CT · Kernel conversion · Image-to-image translation · Contrastive learning · Style transfer

C. Choi and J. Jeong—Contributed equally.

Supplementary Information The online version contains supplementary material available at https://doi.org/10.1007/978-3-031-43999-5_33.

H. Greenspan et al. (Eds.): MICCAI 2023, LNCS 14229, pp. 344–354, 2023.
https://doi.org/10.1007/978-3-031-43999-5_33

1 Introduction

Computed tomography (CT) image is reconstructed from sinogram, which is tomographic raw data collected from detectors. According to kernels being used for CT image reconstruction, there is a trade-off between spatial resolution and noise, and it affects intensity and texture quantitative values [1]. When CT image is reconstructed with sharp kernel, spatial resolution and noise increase, and abnormality can be easily detected in bones or lung. In contrast, with soft kernel, spatial resolution and noise reduce, and abnormality can be easily detected in soft tissues or mediastinum. In other words, CT image is reconstructed depending on what anatomical structure is evaluated. Also, even if the same anatomical structure is analyzed, the kernel being used differs depending on whether it is qualitative or quantitative evaluation. For example, CT images reconstructed with soft kernel is required to evaluate quantitative results for lung instead of sharp kernel. Thus, CT images reconstructed with different kernels would be necessary for accurate diagnosis.

However, once CT image is reconstructed with a specific kernel, sinogram is usually removed because of its large capacity and limited storage. Therefore, clinicians have difficulty to analyze qualitative or quantitative results without CT image reconstructed with different kernels, and this limitation reveals on retrospective or longitudinal studies that cannot control technical parameters, particularly [2]. Besides, there is another problem that patients should be scanned again and exposed to radiation.

Recently, many studies have achieved improvement in kernel conversion [2–5] using image-to-image translation methods [6–13] based on deep learning, especially generative adversarial networks (GANs) [14]. Nevertheless, it remains challenging that translated image should maintain its anatomical structure of source image in medical domain [9]. It is important for quantitative evaluation as well as qualitative evaluation. To solve this problem, we focus on improving maintenance of structure when the source image is translated.

Our contributions are as follows: (1) we propose multi-domain image-to-image translation with generator-guided contrastive learning (GGCL) for CT kernel conversion, which maintains the anatomical structure of the source image accurately; (2) Our proposed GGCL can be easily utilized into other multi-domain image-to-image translation with only changing the discriminator architecture and without adding any additional networks; (3) Experimental results showed that our method can translate CT images from sharp into soft kernels and from soft into sharp kernels compared to other image-to-image translation methods.

2 Method

2.1 Related Work

In deep learning methods for CT kernel conversion, there were proposed methods using convolutional neural networks [2, 3], but they were trained in a supervised manner. Recently, Yang et al. [5] proposed a new method using the adaptive instance normalization (AdaIN) [15] in an unsupervised manner and it showed significant performance, however, this method still has limitations that the target image for the test phase and additional architecture for AdaIN are needed.

Generator-guided discriminator regularization (GGDR) [16] is discriminator regularization method that intermediate feature map in the generator supervises semantic representations by matching with semantic label map in the discriminator for unconditional image generation. It has advantages that we don't need any ground-truth semantic segmentation masks and can improve fidelity as much as conditional GANs [17–19].

Recently, it has been shown that dense contrastive learning can have a positive effect on learning dense semantic labels. In dense prediction tasks such as object detection and semantic segmentation [20, 21], both global and local contrastive learning have been proposed to embed semantic information. Furthermore, it has been demonstrated that patch-wise contrastive learning performs well in style transfer for unsupervised image-to-image translation [12]. This motivated our experiments as it demonstrates that intermediate features can be learned through contrastive learning when learning dense semantic labels.

2.2 Generator-Guided Contrastive Learning

GGDR [16] uses cosine distance loss between the feature map and the semantic label map for unconditional image generation. However, unlike image generation, the generator has a structure with an encoder and a decoder in image-to-image translation [11], and this is quite important to maintain the structure of source image while translating the style of target image. Thus, it might be helpful for discriminator to inform more fine detail semantic representations by comparing similarity using patch-based contrastive learning [12] (see Fig. 1).

Multi-Domain Image-To-Image Translation. We apply generator-guided contrastive learning (GGCL) to StarGAN [6] as base architecture which is one of the multi-domain image-to-image translation model to translate kernels into all directions at once and show stability of GGCL. Basically, StarGAN uses adversarial loss, domain classification loss and cycle consistency loss [13] as follows:

$$\mathcal{L}_D = -\mathcal{L}_{adv} + \lambda_{cls}\mathcal{L}^r_{cls}, \tag{1}$$

$$\mathcal{L}_G = \mathcal{L}_{adv} + \lambda_{cls}\mathcal{L}^f_{cls} + \lambda_{cyc}\mathcal{L}_{cyc}, \tag{2}$$

where $\mathcal{L}_D$ and $\mathcal{L}_G$ are the discriminator and generator losses, respectively. They both have $\mathcal{L}_{adv}$, which is the adversarial loss. $\mathcal{L}^r_{cls}$ and $\mathcal{L}^f_{cls}$ are the domain classification losses for a real and fake image, respectively. $\mathcal{L}_{cyc}$, which is the cycle consistency loss, has an importance for the translated image to maintain the structure of source image.

Patch-Based Contrastive Learning. Our method is to add PatchNCE loss [12] between "positive" and "negative" patches from the feature map of the decoder in the generator and "query" patch from the semantic label map in the discriminator. The query patch is the same location with positive patch and different locations with N negative patches. So, the positive patch is learned to associate to the query patch more than the N negative patches. GGCL loss is the same as PatchNCE loss, which is the cross-entropy loss calculated for an (N + 1)-way classification, and it follows as:

$$\mathcal{L}_{ggcl} = \mathbb{E}_v\left[-\log\frac{\exp\left(v \cdot v^+/\tau\right)}{\exp\left(v \cdot v^+/\tau\right) + \sum_{n=1}^{N}\exp\left(v \cdot v^-_n/\tau\right)}\right], \tag{3}$$

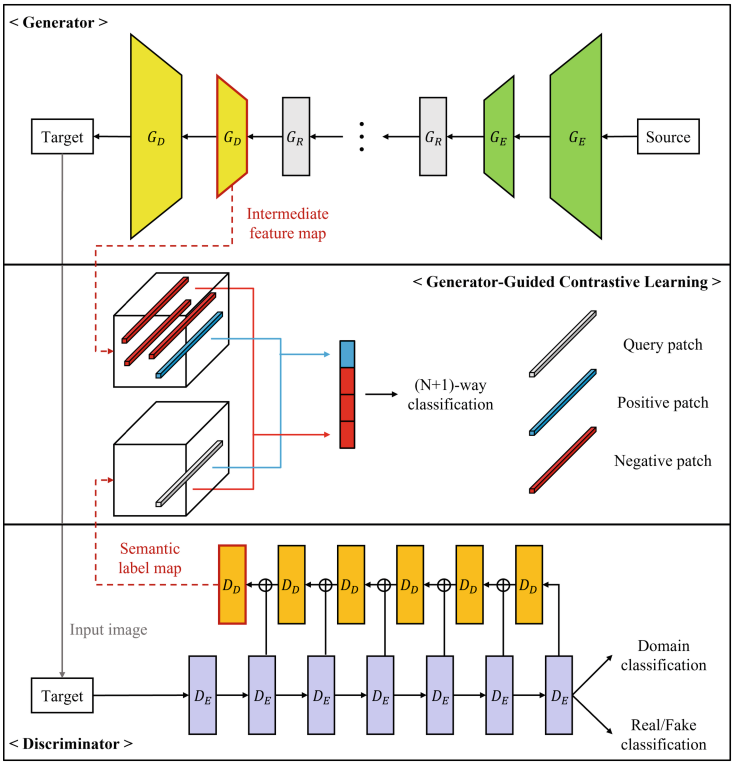

Fig. 1. Overview of generator-guided contrastive learning (GGCL) framework. The proposed method is to add patch-based contrastive learning between the intermediate feature map from the generator and the semantic label map from the discriminator to solve (N + 1)-way classification. G_E, G_R and G_D are the encoder, residual and decoder blocks of the generator, respectively. D_E and D_D are the encoder and decoder blocks of the discriminator, respectively. This method can be applied to any multi-domain image-to-image translation methods.

where v, v^+ and v_n^- are the vectors which are mapped from query, positive and n-th negative patches, respectively. $\tau = 0.07$ is the same configuration as CUT [12]. Since we use the features from the generator and the discriminator themselves, this requires no additional auxiliary networks and no feature encoding process.

Total Objective. GGCL follows the concept of GGDR, which the generator supervises the semantic representations to the discriminator, so it is a kind of the discriminator regularization. Discriminator conducts real/fake classification, domain classification and semantic label map segmentation, so it can be also a kind of the multi-task learning [22]. Our total objective functions for the discriminator and generator are written, respectively, as:

$$\mathcal{L}_D = -\mathcal{L}_{adv} + \lambda_{cls}\mathcal{L}_{cls}^r + \lambda_{ggcl}\mathcal{L}_{ggcl}, \tag{4}$$

$$\mathcal{L}_G = \mathcal{L}_{adv} + \lambda_{cls}\mathcal{L}_{cls}^f + \lambda_{cyc}\mathcal{L}_{cyc}, \tag{5}$$

where λ_{cls}, λ_{cyc} and λ_{ggcl} are hyper-parameters that weight the importance of domain classification loss, cycle consistency loss and GGCL loss, respectively. We used $\lambda_{cls} = 1$, $\lambda_{cyc} = 10$ and $\lambda_{ggcl} = 2$ in our experiments.

3 Experiments and Results

3.1 Datasets and Implementation

Datasets. For train dataset, chest CT images were reconstructed with B30f, B50f and B70f kernels, from soft to sharp, in Siemens Healthineers. We collected chest CT images from 102 (63 men and 39 women; mean age, 62.1 ± 12.8 years), 100 (47 men and 53 women; mean age, 64.9 ± 13.7 years) and 104 (64 men and 40 women; mean age, 62.2 ± 12.9 years) patients for B30f, B50f and B70f kernels from Siemens (see Table 1).

For test dataset, we collected chest CT images from paired 20 (15 men and 5 women; mean age, 67.1 ± 7.4 years) patients for each kernel in Siemens for quantitative and qualitative evaluation.

Table 1. CT acquisition parameters of dataset according to kernels.

	Kernel	Patients	Slices	Age (year)	Sex (M:F)	Slice Thickness	kVp
Test	B30f	102	36199	62.1 ± 12.8	63:39	1.0	120
	B50f	100	32795	64.9 ± 13.7	47:53	1.0	120
	B70f	104	36818	62.2 ± 12.9	64:40	1.0	120
	Kernel	Patients	Slices	Age (year)	Sex (M:F)	Slice Thickness	kVp
Test	B30f	20	6897	67.1 ± 7.4	15:5	1.0	120
	B50f	20	6897	67.1 ± 7.4	15:5	1.0	120
	B70f	20	6897	67.1 ± 7.4	15:5	1.0	120

Implementation Details. We maintained the original resolution 512 × 512 of CT images and normalized their Hounsfield unit (HU) range from [-1024HU ~ 3071HU] to [−1 ~ 1] for pre-processing. For training, the generator and the discriminator were optimized by Adam [23] with $\beta_1 = 0.5$, $\beta_2 = 0.999$, learning rate 1e-4 and the batch size is 2. We used WGAN-GP [24] and set $n_{\text{critic}} = 5$, where n_{critic} is the number of discriminator updates per each generator update. The feature map and the semantic label map were extracted in 256 × 256 size and resized 128 × 128 using averaging pooling. The number of patches for contrastive learning is 64. All experiments were conducted using single NVIDIA GeForce RTX 3090 24GB GPU for 400,000 iterations. We used peak signal-to-noise ratio (PSNR) [25] and structural similarity index measure (SSIM) [26] for quantitative assessment.

Architecture Improvements. Instead of using original StarGAN [6] architecture, we implemented architecture ablations to sample the best quality results, empirically. In

generator, original StarGAN runs 4×4 transposed convolutional layers for upsampling. However, it causes degradation of visual quality of the translated image because of checkerboard artifact [27]. By using 3×3 convolutional layers and 2×2 pixelshuffle [28], we could prevent the artifact. In discriminator, we changed the discriminator to U-Net architecture [29] with skip connection, which consists of seven encoder layers for playing the role of patchGAN [8] and six decoder layers for extracting semantic label map, to utilize GGCL. For each decoder layer, we concatenated the feature from the encoder and the decoder layer with the same size, and ran 1×1 convolutional layer, then ran 2×2 pixelshuffle for upsampling. At the end of the decoder, it extracts semantic label map to compare with the feature map from the decoder layer of the generator. Lastly, we added spectral normalization [30] and leakyReLU activation function in all layers of the discriminator.

3.2 Comparison with Other Image-to-Image Translation Methods

We compared GGCL with two-domain image-to-image translation methods such as CycleGAN [13], CUT [12], UNIT [10] and multi-domain image-to-image translation methods such as AttGAN [7], StarGAN and StarGAN with GGDR [16] to show the effectiveness of GGCL. In this section, qualitative and quantitative results were evaluated for the translation into B30f, B50f and B70f kernels, respectively.

Qualitative Results. We showed the qualitative results of image-to-image translation methods including GGDR and GGCL applied to StarGAN for kernel conversion from Siemens into Siemens (see Fig. 2). For visualization, window width and window level were set 1500 and -700, respectively. While UNIT could not maintain the global structure of the source image and translate the kernel style of the target image, the other methods showed plausible results. However, they could not maintain the fine details like airway wall and vessel in specific kernel conversion, e.g., B50f to B30f, B30f to B50f and B50f to B70f. It could be observed through difference map between the target image and the translated image (see **Supplementary** Fig. 1). GGCL showed stability of translation for kernel conversion with any directions and maintained the fine details including airway wall, vessel and even noise pattern as well as the global structure of the source image.

Quantitative Results. We showed the quantitative results of image-to-image translation methods including GGDR and GGCL applied to StarGAN for kernel conversion from Siemens into the Siemens (see Table 2). In case of two-domain image-to-image translation methods, they showed high PSNR and SSIM performance in translation from B70f into B30f and from B30f into B70f, and UNIT showed the best performance in translation from B30f into B70f. However, they showed low performance in translation into the other kernels, especially soft into sharp, and it indicates that two-domain methods are unstable and cannot maintain the structure of the source image well. In case of multi-domain image-to-image translation methods, their performance still seemed unstable, however, when applying GGDR to StarGAN, it showed quite stable and improved the performance in translation into sharp kernels. Furthermore, when applying GGCL, it outperformed GGDR in translation into many kernels, especially from B30f into B70f and from B50f into B70f.

Fig. 2. The qualitative results of image-to-image translation methods including GGDR and our method for kernel conversion from Siemens into Siemens.

3.3 Ablation Study

We implemented ablation studies about the number of patches, size of pooling and loss weight for GGCL to find out the best performance. We evaluated our method while preserving the network architecture. Ablation studies were also evaluated by PSNR and SSIM. All ablation studies were to change one factor and the rest of them were fixed with their best configurations. The results about the number of patches showed improvement when the number of patches was 64 (see Table 3). The size of pooling also affected the performance improvement, and 2 was appropriate (see **Supplementary** Table 1). Lastly, the results of the loss weight for GGCL showed that 2 was the best performance (see **Supplementary** Table 2).

4 Discussion and Conclusion

In this paper, we proposed CT kernel conversion method using multi-domain image-to-image translation with generator-guided contrastive learning (GGCL). In medical domain image-to-image translation, it is important to maintain anatomical structure of the source image while translating style of the target image. However, GAN based generation has limitation that the training process may be unstable, and the results may be inaccurate so that some fake details may be generated. Especially in unsupervised manner, the anatomical structure of the translated image relies on cycle consistency mainly. If trained unstably, as the translated image to the target domain would be inaccurate, the reversed translated image to the original domain would be inaccurate as well. Then,

Table 2. The quantitative results of image-to-image translation methods including GGDR and our method from Siemens to Siemens.

Method	Sharp to Soft					
	B50f → B30f		B70f → B30f		B70f → B50f	
	PSNR	SSIM	PSNR	SSIM	PSNR	SSIM
CycleGAN	35.672	0.950	44.741	0.974	32.553	0.905
CUT	37.261	0.956	40.394	0.961	34.595	0.910
UNIT	24.545	0.672	44.964	0.979	22.868	0.540
AttGAN	38.685	0.927	37.435	0.900	32.596	0.733
StarGAN	37.262	0.930	36.024	0.903	31.660	0.799
w/ GGDR	47.659	0.987	**45.213**	0.979	**41.391**	**0.950**
w/ GGCL (ours)	**47.831**	**0.989**	44.943	**0.981**	40.332	0.944
Method	Soft to Sharp					
	B30f → B50f		B30f → B70f		B50f → B70f	
	PSNR	SSIM	PSNR	SSIM	PSNR	SSIM
CycleGAN	28.536	0.830	31.544	0.754	30.719	0.758
CUT	35.320	0.902	29.659	0.660	31.402	0.834
UNIT	22.994	0.511	**34.733**	**0.869**	23.288	0.563
AttGAN	32.604	0.753	28.293	0.556	28.662	0.564
StarGAN	31.738	0.836	28.531	0.601	28.527	0.601
w/ GGDR	**41.606**	**0.961**	31.062	0.757	34.547	0.869
w/ GGCL (ours)	41.279	0.958	32.584	0.818	**34.857**	**0.872**

the cycle consistency would fail to lead the images to maintain the anatomical structure. CycleGAN [13], CUT [12] and UNIT [10] showed this limitation (see Fig. 2 and Table 2), but GGCL solved this problem without any additional networks.

The benefit of GGCL was revealed at the translation from soft into sharp kernels. It is a more difficult task than the translation from sharp into soft kernels because spatial resolution should be increased and noise patterns should be clear, so this benefit can be meaningful. Nevertheless, the improvements from GGCL were quite slight compared to GGDR [16] (see Table 2) and inconsistent according to the number of patches (see Table 3). Besides, we did not show results about the different kernels from the external manufacturer. In future work, we will collect different types of kernels from the external manufacturer, and conduct experiments to show better improvements and stability of GGCL.

Table 3. Ablation studies about the number of patches.

Patch Num	Sharp to Soft					
	B50f → B30f		B70f → B30f		B70f → B50f	
	PSNR	SSIM	PSNR	SSIM	PSNR	SSIM
64	**47.831**	**0.989**	44.943	0.981	**40.332**	**0.944**
128	47.788	0.989	**45.318**	0.981	38.484	0.913
256	47.513	0.989	45.282	**0.983**	40.190	0.937
Patch Num	Soft to Sharp					
	B30f → B50f		B30f → B70f		B50f → B70f	
	PSNR	SSIM	PSNR	SSIM	PSNR	SSIM
64	41.279	0.958	32.584	0.818	**34.857**	**0.872**
128	40.294	0.948	31.812	0.781	31.676	0.764
256	**41.375**	**0.958**	**33.208**	**0.830**	34.710	0.867

Acknowledgement. This work was supported by a grant of the Korea Health Technology R&D Project through the Korea Health Industry Development Institute (KHIDI), funded by the Ministry of Health & Welfare, Republic of Korea (HI18C0022) and by Institute of Information & communications Technology Planning & Evaluation (IITP) grant funded by the Korea government (1711134538, 20210003930012002).

References

1. Mackin, D., et al.: Matching and homogenizing convolution kernels for quantitative studies in computed tomography. Invest. Radiol. **54**(5), 288 (2019)
2. Lee, S.M., et al.: CT image conversion among different reconstruction kernels without a sinogram by using a convolutional neural network. Korean J. Radiol. **20**(2), 295–303 (2019)
3. Eun, D.-I., et al.: CT kernel conversions using convolutional neural net for super-resolution with simplified squeeze-and-excitation blocks and progressive learning among smooth and sharp kernels. Comput. Meth. Programs Biomed. **196**, 105615 (2020)
4. Gravina, M., et al.: Leveraging CycleGAN in Lung CT Sinogram-free Kernel Conversion. In: Sclaroff, S., Distante, C., Leo, M., Farinella, G.M., Tombari, F. (eds.) Image Analysis and Processing – ICIAP 2022: 21st International Conference, Lecce, Italy, May 23–27, 2022, Proceedings, Part I, pp. 100–110. Springer International Publishing, Cham (2022). https://doi.org/10.1007/978-3-031-06427-2_9
5. Yang, S., Kim, E.Y., Ye, J.C.: Continuous conversion of CT kernel using switchable CycleGAN with AdaIN. IEEE Trans. Med. Imaging **40**(11), 3015–3029 (2021)
6. Choi, Y., et al.: Stargan: Unified generative adversarial networks for multi-domain image-to-image translation. In: Proceedings of the IEEE Conference on Computer Vision and Pattern Recognition (2018)
7. He, Z., et al.: Attgan: facial attribute editing by only changing what you want. IEEE Trans. Image Process. **28**(11), 5464–5478 (2019)

8. Isola, P., et al.: Image-to-image translation with conditional adversarial networks. In: Proceedings of the IEEE Conference on Computer Vision and Pattern Recognition (2017)
9. Kong, L., et al.: Breaking the dilemma of medical image-to-image translation. Adv. Neural. Inf. Process. Syst. **34**, 1964–1978 (2021)
10. Liu, M.-Y., Breuel, T., Kautz, J.: Unsupervised image-to-image translation networks. Adv. Neural Inform. Process. Syst. **30** (2017)
11. Pang, Y., et al.: Image-to-image translation: methods and applications. IEEE Trans. Multimedia **24**, 3859–3881 (2021)
12. Park, T., et al. (eds.): Computer Vision – ECCV 2020: 16th European Conference, Glasgow, UK, August 23–28, 2020, Proceedings, Part IX, pp. 319–345. Springer International Publishing, Cham (2020). https://doi.org/10.1007/978-3-030-58545-7_19
13. Zhu, J.-Y., et al.: Unpaired image-to-image translation using cycle-consistent adversarial networks. In: Proceedings of the IEEE International Conference on Computer Vision (2017)
14. Goodfellow, I., et al.: Generative adversarial networks. Commun. ACM **63**(11), 139–144 (2020)
15. Huang, X., Belongie, S.: Arbitrary style transfer in real-time with adaptive instance normalization. In: Proceedings of the IEEE International Conference on Computer Vision (2017)
16. Lee, G., et al.: Generator knows what discriminator should learn in unconditional GANs. In: Avidan, Shai, Brostow, G., Cissé, M., Farinella, G.M., Hassner, T. (eds.) Computer Vision – ECCV 2022: 17th European Conference, Tel Aviv, Israel, October 23–27, 2022, Proceedings, Part XVII, pp. 406–422. Springer Nature Switzerland, Cham (2022). https://doi.org/10.1007/978-3-031-19790-1_25
17. Mirza, M., Osindero, S.: Conditional generative adversarial nets. arXiv preprint arXiv:1411.1784 (2014)
18. Park, T., et al.: Semantic image synthesis with spatially-adaptive normalization. In: Proceedings of the IEEE/CVF Conference on Computer Vision and Pattern Recognition (2019)
19. Sushko, V., et al.: You only need adversarial supervision for semantic image synthesis. arXiv preprint arXiv:2012.04781 (2020)
20. Wang, X., et al.: Dense contrastive learning for self-supervised visual pre-training. In: Proceedings of the IEEE/CVF Conference on Computer Vision and Pattern Recognition (2021)
21. Xie, Z., et al.: Propagate yourself: exploring pixel-level consistency for unsupervised visual representation learning. In: Proceedings of the IEEE/CVF Conference on Computer Vision and Pattern Recognition (2021)
22. Zhang, Y., Yang, Q.: A survey on multi-task learning. IEEE Trans. Knowl. Data Eng. **34**(12), 5586–5609 (2021)
23. Kingma, D.P, Ba, J.: Adam: a method for stochastic optimization. arXiv preprint arXiv:1412.6980 (2014)
24. Gulrajani, I., et al.: Improved training of wasserstein gans. Adv. Neural Inform. Process. Syst. **30** (2017)
25. Fardo, F.A., et al.: A formal evaluation of PSNR as quality measurement parameter for image segmentation algorithms. arXiv preprint arXiv:1605.07116 (2016)
26. Wang, Z., et al.: Image quality assessment: from error visibility to structural similarity. IEEE Trans. Image Process. **13**(4), 600–612 (2004)
27. Odena, A., Dumoulin, V., Olah, C.: Deconvolution and checkerboard artifacts. Distill. **1**(10), e3 (2016)
28. Shi, W., et al.: Real-time single image and video super-resolution using an efficient sub-pixel convolutional neural network. In: Proceedings of the IEEE Conference on Computer Vision and Pattern Recognition (2016)

29. Ronneberger, O., Fischer, P., Brox, T.: U-net: convolutional networks for biomedical image segmentation. In: Medical Image Computing and Computer-Assisted Intervention–MICCAI 2015: 18th International Conference, Munich, Germany, October 5–9, 2015, Proceedings, Part III 18. Springer (2015)
30. Miyato, T., et al.: Spectral normalization for generative adversarial networks. arXiv preprint arXiv:1802.05957 (2018)